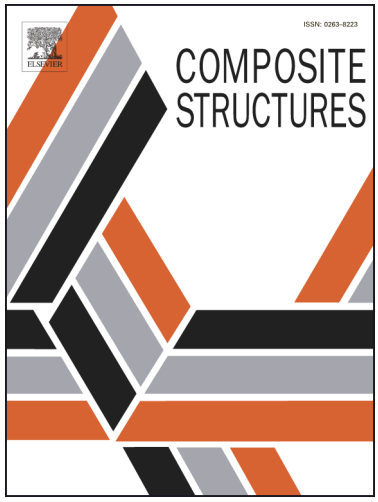

An experimental approach that assesses in-situ micro-scale damage mechanisms and fracture toughness in thermoplastic laminates under out-of-plane loading

H. Wafai, A. Yudhanto, G. Lubineau, R. Yaldiz, N. Verghese

PII: S0263-8223(18)31988-3
DOI: https://doi.org/10.1016/j.compstruct.2018.09.046
Reference: COST 10192

To appear in: *Composite Structures*

Please cite this article as: Wafai, H., Yudhanto, A., Lubineau, G., Yaldiz, R., Verghese, N., An experimental approach that assesses in-situ micro-scale damage mechanisms and fracture toughness in thermoplastic laminates under out-of-plane loading, *Composite Structures* (2018), doi: https://doi.org/10.1016/j.compstruct.2018.09.046

An experimental approach that assesses in-situ micro-scale damage mechanisms and fracture toughness in thermoplastic laminates under out-of-plane loading

H. Wafai[a], A. Yudhanto[a], G. Lubineau[*,a], R. Yaldiz[b], N. Verghese[b]

[a] *King Abdullah University of Science and Technology (KAUST), Physical Sciences and Engineering Division, COHMAS Laboratory, Thuwal 23955-6900, Saudi Arabia*
[b] *SABIC T&I, P.O Box 319, 6160 AH Geleen, The Netherlands*

Abstract

Studying the response of laminated composites under out-of-plane loading routinely involves mechanical tests, such as quasi-static indentation or impact. The phenomenology during these tests is so complex that it is difficult to identify different material properties related to each failure mechanism (damage mode). We aim at providing an experimental approach, which is practical and fast, for assessing the in-situ micro-scale damage mechanism and extracting the fracture toughness in thermoplastic laminates under out-of-plane loading. To this end, we developed a dedicated, micro-scale, three-point bending (micro-3PB) test fitted inside a scanning electron microscope (SEM). In a single experiment, we were able: (i) to assess the initiation of a transverse crack, the transverse crack-to-delamination transition, delamination growth, development of shear-induced microcracks during delamination, and fibrillation, and (ii) to evaluate the effective fracture toughness during transverse cracking and delamination under a representative out-of-plane loading. We used this approach to rank two types of glass fiber-reinforced polypropylene cross-ply laminates, i.e., based on either homopolymer PP (ductile matrix) and copolymer PP (less-ductile matrix), according to their relative fracture parameters. We also performed short edge notch bending (SENB), double cantilever beam (DCB) and end-notch flexure (ENF) to obtain the standard fracture toughness values. We found that the relative fracture toughness values obtained by SENB, DCB and ENF are comparable with that of micro-3PB results. Furthermore, ENF results showed that the delamination process during micro-3PB is dominated by Mode-II fracture.

Keywords: Glass/polypropylene, in-situ, transverse crack, delamination, toughness

1. Introduction

Continuous fiber-reinforced composites based on thermoset matrices have been conventionally used to build lightweight and durable load-bearing structures, such as pipelines, boat hulls, aircraft wings, and fuselages. Recently, thermoplastic-based composites have been increasingly used to produce load-bearing components due to their shorter production cycles, recyclability, improved environmental resistance, and ductility. Thermoplastic composites with improved ductility are particularly promising for impact-prone automotive structures, such as beam stickers, internal door supports, and roofs. These automotive applications call for a detailed understanding of the composite's response under out-of-plane loading.

Multidirectional laminates consisting of plies with various fiber orientations exhibit a complex damage phenomenology under out-of-plane loading. Damage typically starts in the plies that are transversely loaded in-the-plane, beginning with fiber/matrix debonding or microcracking in the bulk matrix and then growing to form transverse cracks [1, 2, 3]. Transverse cracks then initiate delamination between or within plies until final failure [4, 5, 6, 7]. A key step in impact damage is the transition from transverse cracking to delamination. Delamination results from a concentration of stress at the interface due to out-of-plane shearing of existing transverse cracks. Most models have failed to represent the coupling between these two mechanisms correctly. Only models that explicitly introduce cracked surfaces in the micromechanical description [8] or that introduce non-local coupling between plies and interfaces at the meso-scale [9] have successfully captured this coupling. Even so, feeding these models with well-identified material parameters remains challenging.

Observation of damage and crack progression during out-of-plane testing of laminates can be challenging. Testing of plates under quasi-static indentation or impact does not allow the detailed damage mechanism to be monitored during the loading process. Several studies used a simplified test configuration based on a small beam-type specimen under 3- or 4-point

Email address: Corresponding author: gilles.lubineau@kaust.edu.sa (G. Lubineau*,)

bending, in which the fiber and matrix phases could be clearly observed under a scanning electron microscope (SEM) [10, 11, 12, 13, 14]. The specimen configuration enabled the tracking of damage and fracture at the fiber/matrix level and the validation of numerical models. Hobbiebrunken et al. [10] studied transverse cracks in a cross-ply of carbon/epoxy. From the numerical model, they determined that transverse cracks are essentially governed by the interfacial normal strength of the fiber/matrix. Likewise, Canal et al. [11] conducted similar tests on a glass/epoxy beam with notches. They used a finite element simulation of the transverse crack based on the embedded cell method, which revealed that the fracture toughness mainly depended on fiber/matrix interface properties rather than the bulk matrix properties.

Despite progress in this field, how micro-scale test results should be compared with standard fracture test results remains unclear. Certainly, the absolute fracture toughness values obtained by both strategies are expected to be different because the loading configurations and morphologies are different. Yet, an approach to compare the relative values of these strategies need to be further investigated. Additionally, most micro-scale studies were conducted on thermoset-based composites, in which the effect of ductility and viscosity may not be comparable with that in thermoplastic-based composites. Furthermore, characterization of microscopic damage and fracture toughness of thermoplastic-based composites (e.g., on carbon fiber-reinforced PEEK [15, 16, 17, 18, 19, 20, 21] and on glass fiber-reinforced polypropylene [22, 23, 24, 25, 26, 27]) was only conducted under post-mortem conditions, i.e. observing the fractured surfaces of the failed samples. In-situ observations of microscopic damage mechanisms involving multiple types of damage in thermoplastic composites has not been revealed in details.

In this work, we developed a three-point bending test setup for facilitating in-situ micro-scale observation with SEM. The setup allows the transverse cracks and delamination to be isolated and observed at micro-scale where damage features and fracture toughness of respective mechanisms of degradation can be estimated. We used the setup to study the damage behavior of continuous glass fiber-reinforced polypropylene composites made from either homopolymer or copolymer polypropylene. To better understand what should be

the proper interpretation of the fracture toughness obtained by our three-point bending test setup, we carefully compared the relative quantities obtained in our tests with those of standard fracture tests, namely the single edge notch bending (SENB) test for intralaminar Mode-I fracture toughness, and the double cantilever beam (DCB) and end-notched flexure (ENF) tests for Mode-I and Mode-II interlaminar fracture toughness, respectively.

2. Experimental Details

2.1. Materials and manufacture of laminates

We utilized a polypropylene (PP) matrix reinforced with continuous E-glass fibers. To show that our approach is able to rank two material grades with respect to their resilience to out-of-plane loading, we used two PP matrix systems, i.e. homopolymer PP and impact-modified PP (copolymer) designated as "GF-PP" and "GF-IPP", respectively. We reported results on an investigation of GF-IPP earlier [28]. The materials were provided by SABIC in the form of unidirectional tape (0.25 mm thick and 110 mm wide). The fiber volume fractions of GF-PP and GF-IPP were 45% and 41%, respectively. We used a static hot press (Pinette Emidecau Industries 15T) to manufacture GF-PP and GF-IPP laminates. We stacked layers of tape, and inserted them into a custom-made metallic mold (aluminum mold for GF-PP and steel mold for GF-IPP). The consolidation cycle for GF-PP was as follows: under a constant pressure of 6.8 bar, the laminate was heated to 230 °C and dwelled there for 20 min; the temperature was then reduced to room temperature at a rate of 22 °C/min. The consolidation cycle for GF-IPP was similar to that of GF-PP but with constant pressure and dwelling temperature of 7.5 bar and 210 °C, respectively. The dimension of the GF-PP plate was 250×110 mm^2, while that of GF-IPP was 275×110 mm^2.

2.2. Standard fracture test methods

We evaluated Mode-I intralaminar fracture toughness of glass/polypropylene laminates using the single-edge-notch bending (SENB) test following ASTM D-5045 Standard [29]. Here, SENB intralaminar fracture toughness is measured for a transverse crack growing in the thickness direction, to be distinguished from intralaminar fracture toughness based on

the transverse crack growing along the fiber direction [30]. The sample lay-up was $[0]_{30}$ and the dimension was 36 × 7.5 × 4 mm^3. A notch of 3.75 mm was introduced in the middle of the sample using a diamond cutting saw. Then, a razor blade was manually tapped into the notch to create an initial crack of 0.5 mm. We verified that these procedures were giving a consistent dimension among samples. We performed the SENB test using a custom-made three-point bending (3PB) setup installed in the micro tensile/compression machine (Kammrath & Weiss) with a 5-kN load-cell. The loading speed was 1.2 mm/min. We measured the energy derived from the integration of force-displacement curve and considered it as the Mode-I fracture toughness. The integration process was made up to a critical point, which is the maximum force if it falls within 1.00-1.05 C (C is the sample's elastic compliance). Otherwise, the critical load is taken as the load value precisely at 1.05 C. We also included a correction for specimen compression and system compliance as well as pin indentation at the loading point [29].

Mode-I interlaminar fracture toughness of glass/polypropylene was evaluated using the double cantilever beam (DCB) test following ASTM D-5528 Standard [31]. We prepared $[0]_{16}$ samples (240 × 20 × 4 mm^3) containing an initial delamination of 60 mm length made by inserting a non-adhesive tape (70 micron thick) into the specimen midplane. A pair of loading blocks were bonded to one end of the specimen, and was connected to the load cell. We used an Instron 5882 (500 N load cell) to perform DCB test with a loading speed of 5 mm/min. Before testing, we used a razor blade to slightly open the delamination up to 10 mm, and then used Instron's load cell to fully open the delamination up to 60 mm. Once the initial delamination has been fully opened, the mechanical loading was applied and force-displacement curve was recorded. The delamination growth on the specimen edge (containing scales) was captured using PCO SensiCam camera with a frame rate of 0.165 Hz and 0.330 Hz for GF-PP and GF-IPP, respectively. We used higher frame rate for GF-IPP because the delamination growth in GF-IPP was relatively faster than that in GF-PP. Mode-I fracture toughness (G_c) was calculated using a Modified Beam Theory (MBT) described in [31]. We calculated G_c-initiation at the onset where the delamination started to propagate (pop-in), and was observable in the optical images. G_c-propagation was calculated as an

average G_c value in the plateau regime of the R-curve (when G_c value has been stabilized) over a range of delamination length. The range of delamination length was 80-230 mm and 120-225 mm for GF-IPP and GF-PP, respectively. The stable delamination growth in the GF-PP takes longer time than that in GF-IPP due to a more extensive fiber bridging.

Mode-II interlaminar fracture toughness was evaluated using the end-notched flexure (ENF) test based on ASTM D-7905 Standard [32]. The specimen specification used in ENF test was exactly the same with the one used in DCB test: $[0]_{16}$ lay-up, 240 × 20 × 4 mm^3, initial delamination of 60 mm via a non-adhesive tape. The ENF test was conducted using a three-point bending (3PB) setup in an Instron 5882 (10 kN load cell) at the loading speed of 0.5 mm/min. Mode-II fracture toughness was calculated using Compliance Calibration (CC) method where the maximum load was considered as a critical load [32]. In CC method, we first positioned one of the 3PB supporting pins at three distances sequentially, i.e. 20 mm, 40 mm and 30 mm, while we recorded the force-displacement curves. We first positioned one of the supporting pins 20-mm away from the crack tip, loaded the specimen and obtained the force-displacement curve. Next, we positioned the pin 40-mm away from the crack tip, loaded the specimen again and obtained the force-displacement curve. These first two loadings were conducted up to one half of the expected maximum load (which was calculated by an equation provided in ASTM D-7905) to guarantee elastic loading/unloading without introducing any crack propagations. Finally, we positioned the pin 30-mm away from the crack tip, and loaded the specimen until the load dropped due to crack propagation. The unloading force-displacement data (now, with a new crack length) was also recorded to generate the unloading compliance. We then derived the new crack length by comparing this unloading compliance with the compliance calibration (CC) obtained from the three tests at 20, 30 and 40 mm. Once the new crack length has been calculated, the value of G_c-initiation is calculated using the maximum load value (at 30 mm), the new crack length, and the compliance calibration. This entire process was then repeated for the second time, starting with the crack that has been propagated in the first round, to obtain G_c-propagation. For GF-IPP, the crack length after the first round of compliance calibration (CC-1) was ranging between 47 and 48.5 mm. For GF-PP, CC-1 was ranging between 41.5 and 52.5

mm. In the second round of compliance calibration (CC-2), the new crack length in GF-IPP was ranging between 48.2 and 57.9 mm. Unfortunately, we could not obtain the result of CC-2 for GF-PP because all samples were failed by local buckling under the loading pin before the crack managed to propagate.

2.3. Micro-scale three-point bending test method

We proposed to use the three-point bending test method to isolate the growth of two principal damage mechanisms at the micro-scale, i.e., transverse cracking and delamination, under a scanning electron microscope (SEM). Hereafter, we call the method micro-scale 3PB or "micro-3PB". In doing so, we selected an unsymmetrical cross-ply $[0_4/90_8]_T$ laminate. This selection ensured that the neutral axis (calculated based on the longitudinal and transverse properties of GF-IPP [33]) of the beam was in the $[0]_4$ plies, thus keeping the transverse crack and delamination entirely under tension state. The observation at micro-scale was made possible with a relatively small specimen of 40 × 6 × 3 mm^3 shown in Fig. 1a. A notch of 1 mm (a_0) was created in the middle of $[90]_8$ plies using 300 μm thick diamond saw in a controlled way. We did not make a pre-crack in this specimen. This notch was sufficient to act as a geometrical discontinuity in [90] plies, and to trigger the expected position of the transverse crack. a_0 is chosen to ensure stable crack propagation; we provide the numerical procedure for choosing a_0 in the Appendix. This notch ascertained the initiation of single, stable transverse crack in [90] plies, which would reach the transition point and branch into delamination at the [0/90] interface (Fig. 1b). [0] plies, which were in direct contact with the loading pin during the micro-3PB test, also ensured no premature crushing in [90] plies. It should be noted that this unsymmetrical lay-up created a post-manufacturing curvature due to thermal residual stresses. However, we validated that the curvature was negligible because the residual deflection associated with the residual stresses was small (less than 1%) compared to the maximum displacement applied during the test. To aid the observation under scanning electron microscope (SEM), one of the specimen edges was wet-polished using rotating sandpaper (Struers TegraPol-35) and then sputtered using a 5-nm layer of Au/Pd. Two ends of the specimen were wrapped using a conductive

aluminum tape to guarantee an electrical discharge during SEM analysis.

Figure 1: (a) Schematic of a $[0_4/90_8]_T$ test sample (all dimensions are in mm) under three-point bending, (b) SEM image showing layer-like fiber arrangement in the laminate, notch location and anticipated damage mechanism.

We performed micro-3PB tests on GF-PP and GF-IPP specimens using a micro tensile/compression machine (5 kN load cell, Kammrath & Weiss, see Fig. 2a) where we

designed a 3-pin fixture fitted into the grips of the machine (Fig. 2b). The entire setup was installed inside SEM machine (Quanta 600F, FEI) for an in-situ damage observation. We applied the load up to failure with the loading speed of 1.2 mm/min. SEM images were obtained continuously with a frame rate of 1 frame/sec. We then used the SEM images to measure the crack length. The procedure to calculate the fracture toughness is discussed in Section 3.3.

3. Results and Discussion

3.1. Force-displacement curves from micro-3PB test

The force-displacement curves of GF-PP and GF-IPP (five samples each) from the micro-3PB test is shown in Fig. 3a. The scatter in the curves indicates that the mechanical response was partly affected by the geometrical variation in the sample width B and thickness h. After normalizing the force with the moment of inertia I of [0] ply ($I_{[0]} = Bh_{[0]}^3$; $h_{[0]}$ is thickness of [0] plies of each corresponding sample), Fig. 3b shows that the scatter in the curves is improved. The fact that GF-PP and GF-IPP do not produce a significant difference in terms of force-displacement response is ascribed to the high bending stiffness of [0] plies that controls the global mechanical response. Albeit improved, the data scatter in Fig. 3b was also influenced by the variation of local fiber volume fraction, fiber waviness and fracture process at the micro-scale, which affected the overall response of such a small specimen. The load drop at 10 N (Fig. 3a) or 2 N/mm^4 (Fig. 3b) is strongly related to the initiation and propagation of transverse crack. The initial drop was caused by fact that the transverse crack grows quite quickly and its position is also relatively far from the neutral axis, which affects the bending response. The end of the load drop, which is characterized by the recovery of stiffness, is related to the propagation stage where the growth of transverse crack is slowing down as it enters the rich-resin area close to the interface (transition point).

3.2. Damage mechanism from micro-3PB test

Fig. 4 shows the SEM images illustrating the growth of transverse crack and delamination in GF-PP and GF-IPP. The sequence of damage, which is similar for both GF-PP and GF-

Figure 2: (a) The experimental setup, where the Kammrath & Weiss machine is fixed inside SEM using a special adapter; the specimen is then placed on the 3-point stage such that the initial crack is aligned with the loading pin, (b) custom-designed 3-point bending fixture to be fitted in the micro-tensile machine. The design allows the spacing between the pins to be changed.

IPP laminates, can be described as follows: (i) damage initiates from the initial crack tip in [90] ply until a complete transverse crack was formed, (ii) delamination initiates at the intersection (transition point) between the transverse crack and the [0/90] interface, (iii) delamination grows along [0/90] interface. The growth of the delamination was symmetrical

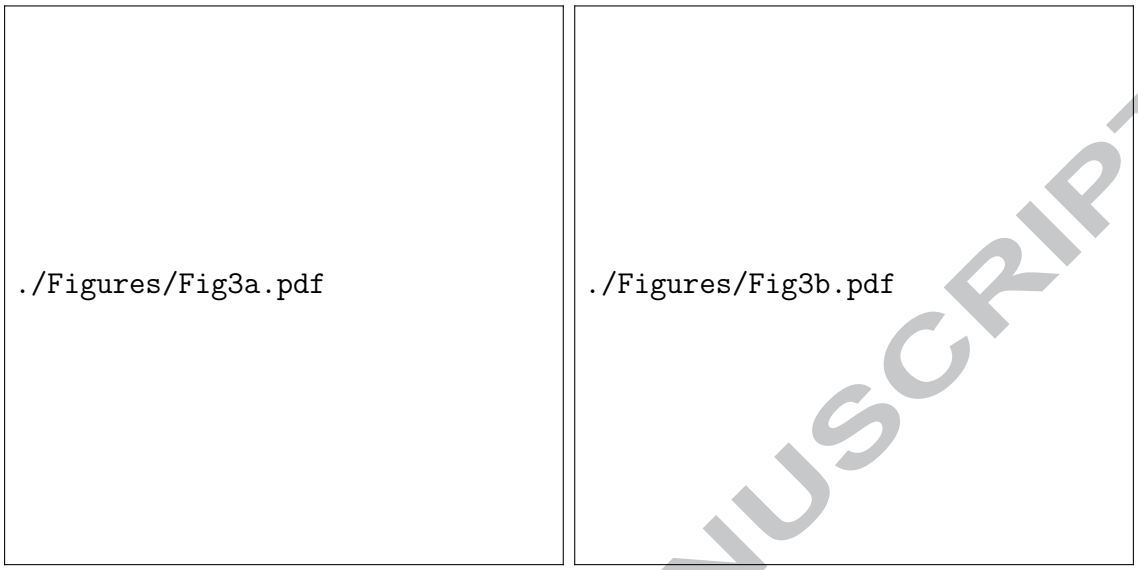

(a) (b)

Figure 3: Micro-3PB test results of GF-PP (blue line) and GF-IPP (black line): (a) force-displacement, (b) normalized force-displacement.

in all tested samples.

The detailed characteristic of transverse crack, taking GF-IPP as an example, is shown in Fig. 5. After the damage was initiated at the tip of the initial crack, the fiber-matrix debonding initiated in the fiber-rich layers where the stress concentration between fibers is the highest. Afterward, the coalescence of cracks over resin-rich layers ensued. In this regard, resin-rich layer temporarily halted the transverse crack growth, while fiber/matrix debonding in the adjacent fiber-rich layer initiated ahead of the transverse crack tip. A similar observation was also reported for ductile polyurethane-based composites [34]. Another feature of the transverse crack was the crack opening that is bridged by the matrix fibrillation, which was not observable in the thermoset composites [10, 11, 12]. The fibrillation suggested that the crack was formed by the crazing mechanism due to disentanglement of polymeric chains [35].

Once the transverse crack reached the [0/90] interface, its growth was paused (see Figs. 6a and d for GF-PP and GF-IPP, respectively). Then, delamination ensued at the interface either by microcracks in the resin-rich layer or by fiber/matrix debonding at the boundaries

Figure 4: SEM image sequence illustrating the damage growth in GF-PP (left) and GF-IPP (right) at similar intervals of pin displacement.

of the fiber-rich layers. Delamination is characterized by the formation of shear-induced microcracks (hackles at approximately 45° with respect to the [0] ply in the matrix phase) and fibrillations inside these microcracks, which are shown in Figs. 6b and e. These damage characteristics indicate a mixed-mode behavior of Mode-I and Mode-II: (i) microcrack opening and fibrillation indicate Mode-I fracture and crazing, respectively; (ii) shear-induced microcracks signify the existence of Mode-II fracture [36]. These shear-induced microcracks, which have also been observed in mineral-filled epoxy with thermoplastic inclusions [37], seem to be dependent on the thickness of the resin interlayer and the distribution of the adjacent fibers [38]. Finally, the delamination continued until the [0] ply failed by the buckling mode near the loading pin (Figs. 6c and f).

Figure 5: SEM observations of crack initiation in a GF-IPP after stopping the test at $\delta = 150\,\mu m$.

We used the damage phenomenology described above to differentiate the two glass/polypropylene types. Here, the initiation and propagation of transverse cracks (which are mainly controlled by the interfiber distance [39] rather than by the matrix toughness) were similar for both GF-PP and GF-IPP. A clear difference between GF-PP and GF-IPP was observed when the transverse crack reached [0/90] interface and the delamination began to increase. At this stage, GF-IPP exhibits a longer delamination than GF-PP by a factor of two (the damage measurement is described in Section 3.4). The thickness of the interlayer is similar

Figure 6: SEM images of damage mechanisms in GF-PP (a-c) and GF-IPP (d-f) during transverse crack, delamination and failure stages.

for both GF-PP and GF-IPP, which is around 97 μm. This difference with respect to delamination is therefore mainly attributed to the effect of the different matrix ductility and toughness between GF-PP and GF-IPP. Finally, the strenuous transition from transverse cracking to delamination in GF-PP suggests that GF-PP should perform better than GF-

IPP in terms of delamination resistance at the larger scale, e.g., during DCB and ENF tests (as later shown), or during the quasi-static indentation (QSI) test [40].

3.3. Fracture toughness from the micro-3PB test

We used our test to identify the effective fracture toughness, G_c, that includes the dissipation originating from all possible mechanisms of dissipation (volume mechanisms such as plastic deformation and crazing or surface mechanisms such as cracking). Indeed, dissipation in the bulk of the material always exists. Standard fracture tests are designed to minimize the bulk dissipation to identify the surface energy related to fracture. However, in a pragmatical approach such as the one we are developing here, it is useful to evaluate the effective fracture toughness including the bulk dissipation. Indeed, the test comes close to a real out-of-plane configuration and total dissipation is much better identified under such conditions. The strain energy of a system, $W(F, \delta)$, can be calculated as follows:

$$W = \frac{1}{2} F\delta \tag{1}$$

and the fracture toughness (equal to the strain energy release rate during propagation) is given as:

$$G_c = -\frac{\partial W}{\partial A} = -\frac{1}{2B}\frac{\partial}{\partial a}\{F\delta\} \tag{2}$$

where force F and displacement δ were obtained from the PC connected to the Kammrath & Weiss machine; A is crack area ($A = a.B$), B is specimen width, a is measured crack length. G_c can be directly calculated from the slope of curve-fitted line correlating ($F\delta/2B$) and a. We separately calculated G_c based on the crack length a measured in the transverse crack and delamination phases.

Fig. 7 shows the SEM image used for measuring total crack length, consisting of initial crack, transverse crack, and delamination (always symmetrical). The results correlating the crack length and pin displacement for GF-PP and GF-IPP are shown in Fig. 8. We found that GF-PP and GF-IPP experience similar transverse crack progressions, but differ in terms of delamination. As a result, the fracture toughness, G_c, during transverse cracking of GF-PP was similar to that of GF-IPP. On the other hand, as shown in Table 1, G_c of GF-PP

during delamination was three to four times higher than that of GF-IPP. The relative value of G_c^A/G_c^B for each fracture mode is also given in Table 1 where G_c^A and G_c^B are fracture toughness values for GF-PP (Material-A) and GF-IPP (Material-B), respectively.

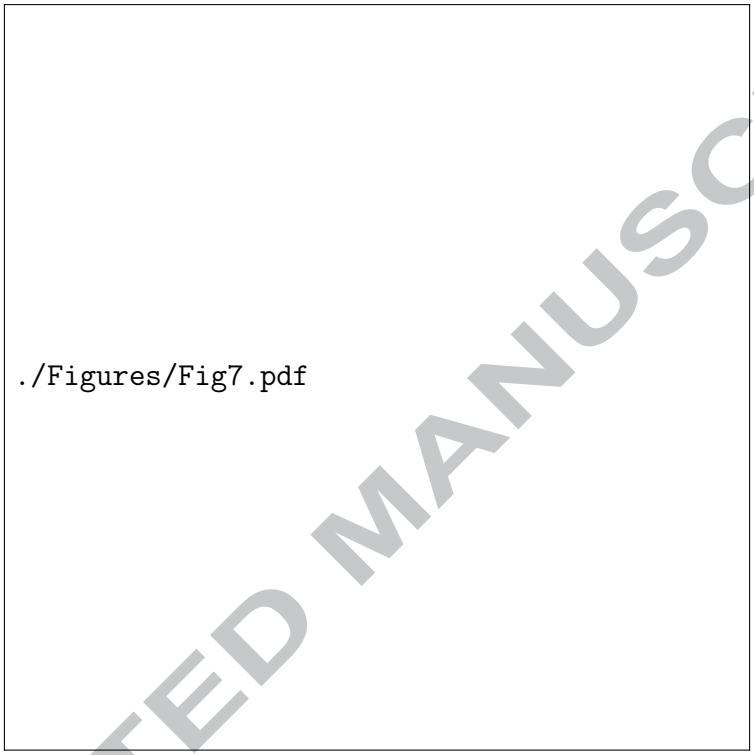

Figure 7: Crack measurement based on SEM image consisting of notch, transverse crack and delamination phases.

Table 1: Intralaminar and interlaminar fracture toughness in kJ/m^2 of glass/polypropylene obtained by micro-3PB.

Fracture mode	Stage	G_c^A (GF-PP or Material A)	G_c^B (GF-IPP or Material B)	Relative value G_c^A/G_c^B
Intralaminar	Transverse crack	0.22 ± 0.03	0.19 ± 0.05	1.2
Interlaminar	Delamination	3.63 ± 0.99	1.07 ± 0.16	3.4

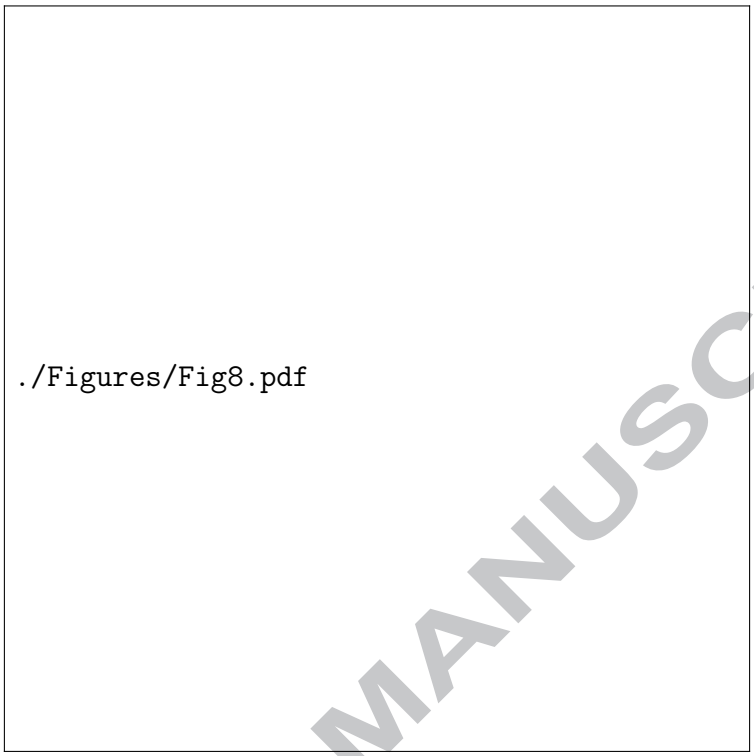

Figure 8: Micro-3PB result of crack length and pin displacement for GF-PP and GF-IPP.

3.4. Contribution of matrix deformation on energy dissipation

We further performed incremental micro-3PB test to measure the contribution of matrix deformation on the energy dissipation during the damage process (transverse crack and delamination). Here, we performed a set of load/unload tests on both materials with incrementally increasing displacement (100, 200, 300, 400, 500, 1000, 1500, and 2000 μm). We tested five specimens for each material system. Typical load/unload curves for GF-PP and GF-IPP are shown in Fig. 9. We then measure the crack length, residual displacement (displacement onset in the unloading phase when the force is zero), stiffness degradation and energy dissipation at each cycle. The stiffness of each cycle S_i was calculated as a slope between 1 N and 5 N in the loading phase of force-displacement curve. The range of 1-5 N represents the first cycle where the response is still elastic and does not feature any crack evolution. Then, stiffness degradation d_i is calculated as follows:

$$d_i = 1 - \frac{S_i}{S_0}, \tag{3}$$

where S_0 is a reference, undamaged stiffness taken at the initial loading phase. Note that the stiffness here is not a material property, but a sample-specific quantity. This approach is deemed reasonable in order to decouple the contribution of elastic/damage and plastic parts during material degradation. It should be noted that the damage does not represent a material damage as in mesoscale damage mechanics approach. Instead, it is an equivalent damage that can be represented by a global stiffness reduction of sample at macro-scale. Finally, the energy dissipation is calculated from the hysteresis area of the load/unload curves.

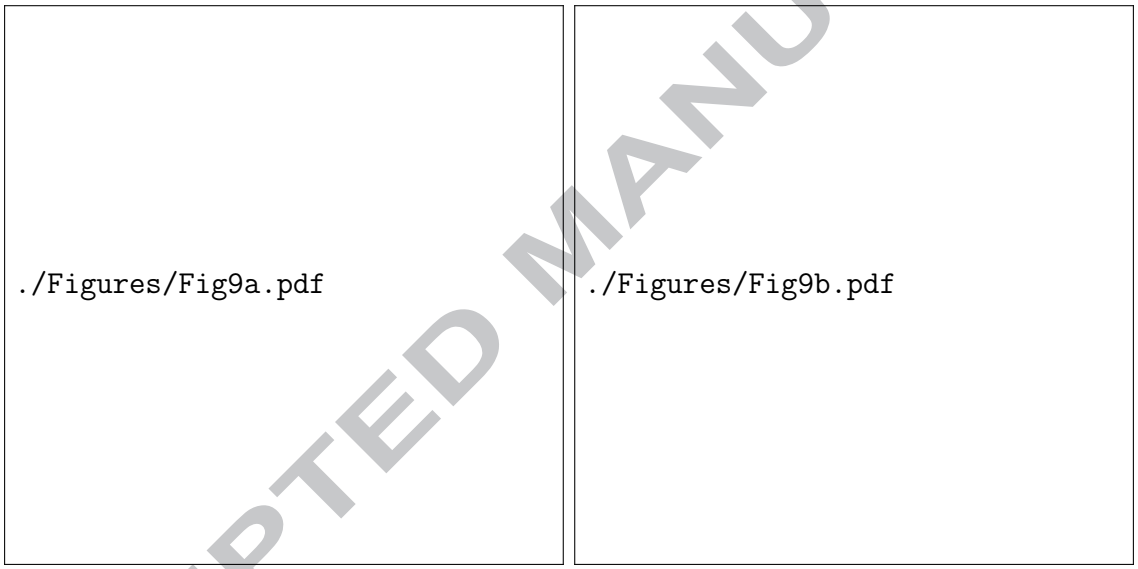

Figure 9: Typical force-displacement curves of load/unload tests of (a) GF-PP, (b) GF-IPP.

During the first phase (propagation of the transverse crack), GF-IPP and GF-PP exhibit similar residual displacements and stiffness degradations. The contribution of matrix deformation is therefore negligible during this phase, which is mainly governed by the inter-fiber distance. During the second phase (propagation of the delamination), the interpretation is quite different. GF-PP exhibits a greater cumulative residual displacement as compared to GF-IPP (see Fig. 10a), and it experiences a sharp increase in residual displacement during delamination (see Fig. 10b). The trend of dissipated energy in GF-PP and GF-IPP as shown

in Figs. 10c-d follows with the trend of residual displacement. GF-PP globally dissipates more energy than GF-IPP does and this dissipation is realized through both the increase in crack length (but limited) and the increase in residual displacement, which together suggest a strong contribution by the matrix deformation. Here, the matrix deformation could be due to viscoelasticity or plasticity, which is usually shown by some relaxation after the test has been paused. The effective toughness identified during the delamination phase globally encompasses all these effects. Further study of the contribution of viscoelasticity on the matrix deformation is left to future research.

3.5. Standard fracture test results

Force-displacement curves of SENB shown in Fig. 11a indicates that Mode-I intralaminar fracture response, i.e., transverse crack behavior, of GF-PP and GF-IPP is similar. The scatter in Fig. 11a was influenced by the variation of specimen's geometry (width, thickness), fiber volume fraction of small specimen, and transverse crack process at micro-scale, which is induced by the fiber distribution. DCB test results, i.e. force-displacement, for GF-PP and GF-IPP are shown in Fig. 11b. In such opening mode (Mode-I), GF-PP is significantly tougher than GF-IPP, which typically corresponds to a slower crack progression. Force-displacement curves of ENF test for GF-PP and GF-IPP are shown in Fig. 11c. Similar to Mode-I, force-displacement curves from Mode-II ENF test show that GF-PP achieved a higher peak force compared to GF-IPP, which suggests a higher Mode-II fracture toughness.

After measuring the crack length for each fracture test, we calculated the corresponding fracture toughness G_c and tabulated the test results in Table 2. Mode-I intralaminar fracture toughness of GF-PP is around 10% higher than that of GF-IPP, indicating that PP type does not significantly affect the transverse crack phase of glass-reinforced polypropylene. Mode-I interlaminar fracture toughness of GF-PP is 3.5 and 6.4 times higher than that of GF-IPP during initiation and propagation phases, respectively, due to its higher matrix ductility and extensive fiber bridging (shown in Fig. 12). In terms of the absolute magnitude, our G_c is comparable with the value reported in Refs. [22, 25, 26, 27]. Mode-II interlaminar fracture toughness of GF-PP during initiation is also higher than that of GF-IPP. Likewise, our G_c

of ENF tests are comparable with those provided in Refs. [23, 24, 25, 27]. Unfortunately, we could not obtain G_c during propagation because all ENF samples failed by buckling during the second compliance calibration round, even before reaching the force necessary to propagate the delamination.

Table 2: Intralaminar and interlaminar fracture toughness in kJ/m^2 of glass/polypropylene obtained by SENB, DCB and ENF.

Fracture mode	Test method	Stage	G_c^A (GF-PP or Material-A)	G_c^B (GF-IPP or Material-B)	Relative value G_c^A/G_c^B
Mode-I intralaminar	SENB	-	0.37 ± 0.07	0.33 ± 0.04	1.1
Mode-I interlaminar	DCB	Initiation	0.74 ± 0.05	0.21 ± 0.02	3.5
Mode-I interlaminar	DCB	Propagation	1.98 ± 0.13	0.31 ± 0.02	6.4
Mode-II interlaminar	ENF	Initiation	3.92 ± 0.41	0.92 ± 0.02	4.3
Mode-II interlaminar	ENF	Propagation	-	0.91 ± 0.08	-

3.6. Relative comparison between micro-3PB and standard tests

We compared the micro-3PB and standard fracture test results. The relative values of G_c^A/G_c^B for each fracture mode from the micro-3PB and standard tests are given in Tables 1 and 2, respectively. This comparison yielded the following observations:

- During the transverse crack phase, the G_c^A/G_c^B obtained by micro-3PB is comparable with that obtained by SENB, i.e. G_c^A/G_c^B of micro-3PB and SENB is 1.2 and 1.1, respectively. The relative value of micro-3PB during the transverse crack phase seems to be able to approximate the SENB result. However, absolute G_c values of GF-PP and GF-IPP obtained by micro-3PB (0.22 and 0.19 kJ/m^2, respectively) are lower than those obtained by SENB (G_c of GF-PP and GF-IPP is 0.37 and 0.33 kJ/m^2, respectively). The [0] plies in $[0_4/90_8]_T$ of the micro-3PB test specimen dissipate less energy during the growth of the through-thickness transverse crack in the [90] plies

as compared to the thick [90] samples of the SENB test. For such materials in which dissipation in the resin might be significant, using the micro-3PB configuration is clearly a good way to reduce the contribution of the dissipation in the resin when identifying the fracture toughness of transverse cracking.

- During the delamination phase, the relative value of G_c obtained by the micro-3PB test is comparable with that of DCB at the initiation phase (G_c^A/G_c^B of micro-3PB and DCB at initiation is 3.4 and 3.5, respectively), indicating that we could use the micro-3PB results to rank the materials based on the relative Mode-I fracture parameters. Also, the absolute value of G_c obtained by the micro-3PB test during delamination is closer to G_c of Mode-II (initiation) from the ENF test rather than G_c of Mode-I (initiation) from the DCB test. This can be explained by the important contribution of Mode-II during the propagation of the delamination in the micro-3PB sample (see Fig. 14c in the Appendix). This is also consistent with the observation of intense shear-induced microcracks in the SEM observations. However, we again emphasize that the identified toughness is a globalizing parameter corresponding to the specific Mode-I/Mode-II ratio for the chosen micro-3PB configuration.

We suggest that the proposed micro-3PB test is suitable to rank the relative fracture toughness of different materials (where the measurement on a reference material is required). The specimen's interface of [0/90] studied in our micro-3PB test represents a classical interface, which could be useful in probing the transition from transverse cracking to delamination under out-of-plane loading, such as is done by the lay-up in Ref. [40]. Obviously, our micro-3PB test needs to be evaluated for other interfaces given that Allix et al. [41] and Daghia et al. [42] have demonstrated that the relative orientation of the plies at the interface can have a major influence on interlaminar fracture properties. We believe that our micro-3PB test could provide configuration-specific material parameters that are needed, for instance, in out-of-plane impact models.

4. Conclusions

An in-situ experimental approach based on three-point bending setup was developed to assess the micro-scale fracture behavior of glass/polypropylene laminates under scanning electron microscope (SEM). We applied this approach to study the fracture behavior of homopolymer-based and copolymer-based glass-reinforced polypropylene (namely, GF-PP and GF-IPP, respectively) laminates. We found that homopolymer and copolymer PP, which represent ductile and less-ductile matrices, produce similar transverse crack behavior in glass/polypropylene system, which shows the dominance of inter-fiber stress concentration over matrix toughness during the transverse cracking process. On the other hand, GF-PP is more resistant to delamination (correspondingly, exhibits a higher fracture toughness) than GF-IPP. An evidence of mixed-mode (Mode-I and Mode-II) fracture behavior in the resin-rich layer, e.g. shear-induced microcracks and fibrillation, was attained by the micro-3PB and SEM.

In a single experiment, our micro-3PB test is effective in revealing the micro-scale features of transverse cracks, transition points and delamination. This approach is also practical in ranking the materials based on their relative fracture toughness (during both transverse cracking and delamination). It is potentially a cost-effective approach given that a large number of materials (with a relatively small sample size) can be categorized based on their fracture behaviors and the relative magnitude of fracture toughness.

Acknowledgments

The authors would like to thank the Saudi Basic Industries Corporation (SABIC) for funding this research under Grant Agreement number RGC/3/2050-01-01 and providing the materials, as well as scientific support. This research was also partially supported by King Abdullah University of Science and Technology (KAUST) Baseline Research Funds under award number BAS/1/1315-01-01.

Appendix A. Finite element analysis of initial crack length

A1. Introduction

The numerical approach used to choose a notch length, $a_0 = 1\,mm$, is given here. a_0 was selected to ensure that the transverse crack remained relatively stable during displacement-controlled micro-3PB.

A2. Governing equations

Proportionality coefficient α_a is a scalar that depends on the system geometry (length L, width B, thickness h as well as the notch length a) and material parameters. The relation between strain energy of a system and the proportionality coefficient is expressed as follows

$$\exists \alpha_a; W(a,\delta) = \alpha_a \delta^2 \tag{4}$$

where δ is loading pin displacement, $W(a,\delta)$ is strain energy of a system. The strain energy release rate G for a linear elastic system under displacement control is defined as follows:

$$G = -\frac{\partial U}{\partial A} = -\frac{\partial W}{\partial A} = \frac{1}{B}\frac{\partial}{\partial a}\left\{-\alpha_a(a)\delta^2\right\} \tag{5}$$

where U is the potential energy of a system, A is the crack area ($A = a.B$). For a crack that is propagating in a stable manner, we assume that

$$G = G_c \tag{6}$$

where G_c is critical energy release rate or fracture toughness. Finally, we can establish an expression that defines the relation between crack length a, pin displacement δ at any given critical energy release rate G_c as follows:

$$\delta = \sqrt{\frac{-BG_c}{\partial \alpha_a / \partial a}} \tag{7}$$

A3. Finite element model and procedure

We performed finite element (FE) analysis of $[0_4/90_8]_T$ beam under 3PB using ABAQUS Standard. The beam was modeled as two homogeneous parts representing the elastic properties of $[0]_4$ and $[90]_8$ plies. Fig. 13 shows the finite element mesh, boundary conditions,

loading point and crack path. Linear elastic and 2D plain strain conditions were assumed during simulation. A series of simulations was performed in ABAQUS Standard using FE models with various notch length, starting from $a = 0$ mm up to $a = 8$ mm with an incremental crack length of $\Delta a = 0.25$ mm. One notch length in each model was created by separating the corresponding nodes (the crack does not actually grow during the simulation). The maximum length of 8 mm consists of notch length of 1 mm, transverse crack length of 1 mm and delamination length of 6 mm; the delamination developed on both sides of the model after the transition point. The displacement control in a ramp-mode was applied equally to all simulations from 0 up to $\delta_{max} = h/10 = 0.3$ mm in order to maintain a small displacement condition and consequently geometrical linearity. It should be noted that the non-linear geometry option in ABAQUS was switched-off after verifying that it has a negligible effect on the results.

Remark. This numerical analysis is certainly a coarse approximation based on the assumption that the toughness is constant throughout the crack path, especially during transverse crack-to-delamination transition. The approximation was made to guess the initial notch length, which produced a stable crack propagation. By comparing the numerical result with the experiments, we found that the selected notch length indeed resulted in a stable crack propagation.

A4. Finite element results

As a first step, we verified our assumption of using computationally-efficient 2D plane strain elements in the FE model. We compared the strain energy W over the crack length a for 2D plane strain, 2D plane stress and 3D full stress depicted in Fig. 14a. It is found that they produced similar strain energy values over the studied crack length, showing that the selected elements have a negligible though-thickness edge effect.

We then calculated coefficient α_a using Eq. 4. $\partial\alpha_a/\partial a$ was obtained numerically using central difference method. The relation between crack length a and pin displacement δ was calculated using Eq. 7. Fig. 14b depicts the solution for a hypothetical value of critical energy release rate $G_c = 1$ kJ/m^2 (for both the transverse crack and delamination). The

curve indicates that transverse cracking is unstable if a_0 is less than 1 mm (half of [90] plies thickness). This threshold does not change for different values of G_c. Hence, a_0 of all our samples was set to 1 mm regardless of the material types.

We further used the FE models to study the mode-mixity during the transverse crack and delamination phases by adopting the Virtual Crack Closure Technique (VCCT) [43]. Fig. 14c presents the percentage of fracture modes, i.e., Mode-I and Mode-II, along crack length a. In the transverse crack phase ($1 \leq a \leq 2$ mm), the fracture mode is purely Mode-I. In the delamination phase ($a > 2$ mm), the fracture mode gradually changes from purely Mode-I into a mixed-mode fracture at $a = 3$ mm, and the fracture mode reaches a stable ratio of approximately 75% of Mode-I and 25% of Mode-II. The percentage of fracture mode shown in Fig. 14c reaches a plateau regime after 2 mm crack length, indicating that the ratio of Mode-I and Mode-II remains constant.

(a)

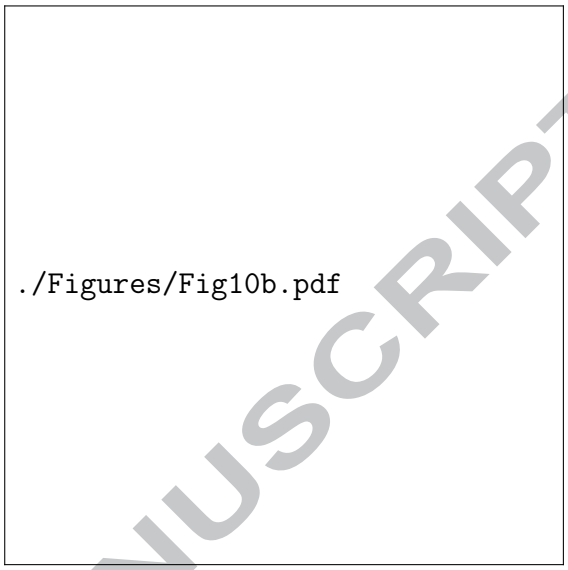

(b)

(c)

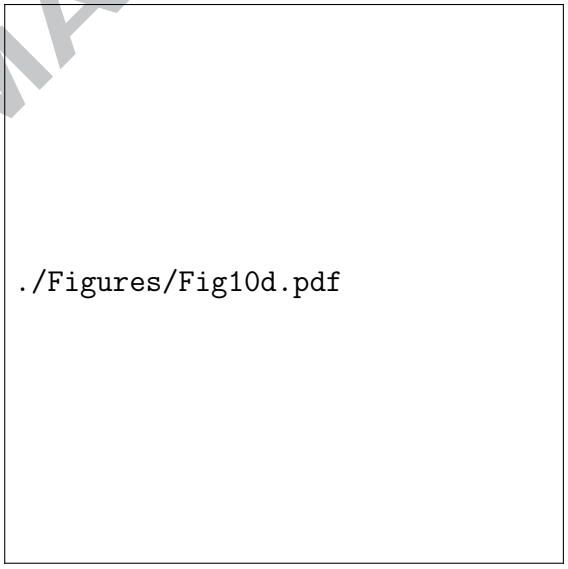

(d)

(e)

Figure 10: (a) Cumulative residual displacement and maximum pin displacement, (b) cumulative residual

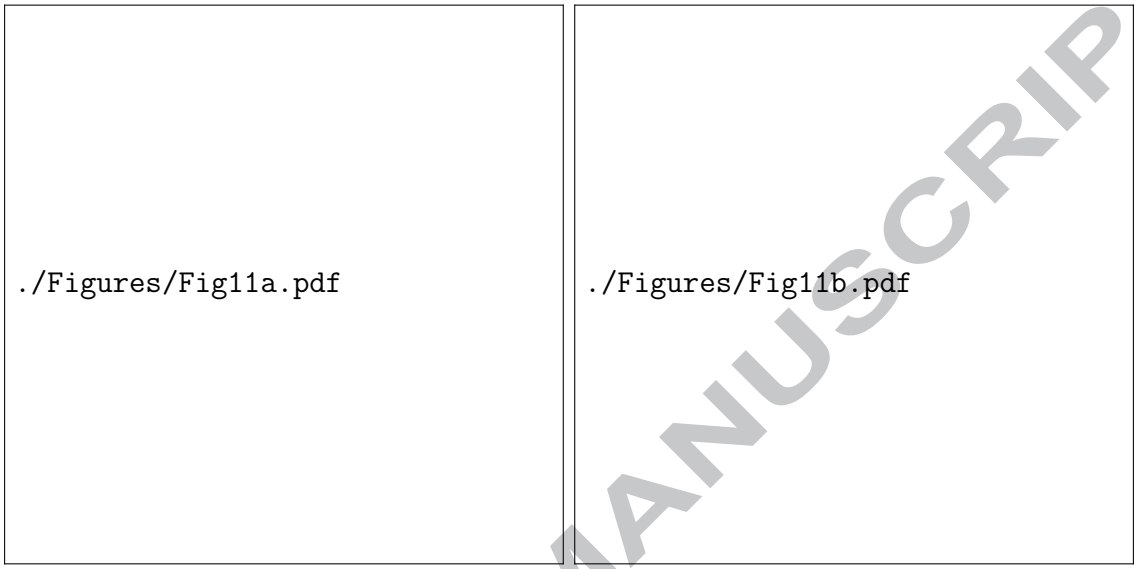

(a) (b)

(c)

Figure 11: Force-displacement curves obtained from standard fracture tests: (a) SENB for Mode-I intralaminar, (b) DCB for Mode-I interlaminar, (c) ENF for Mode-II interlaminar.

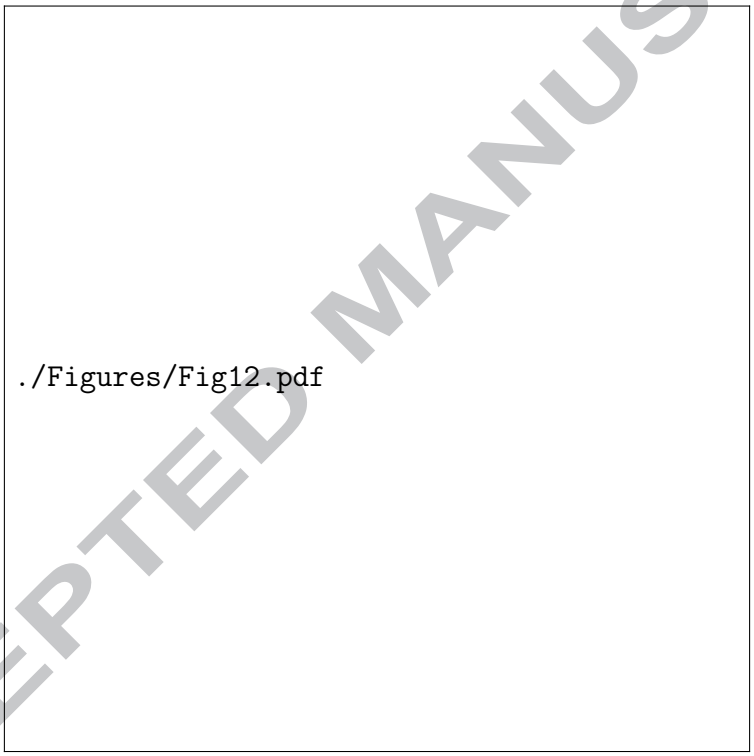

Figure 12: Fiber bridging during DCB tests in (a) GF-PP and (b) GF-IPP.

Figure 13: Finite element model of glass/polypropylene laminate with $[0_4/90_8]_T$ under three-point bending condition where crack paths for transverse crack and delamination are outlined.

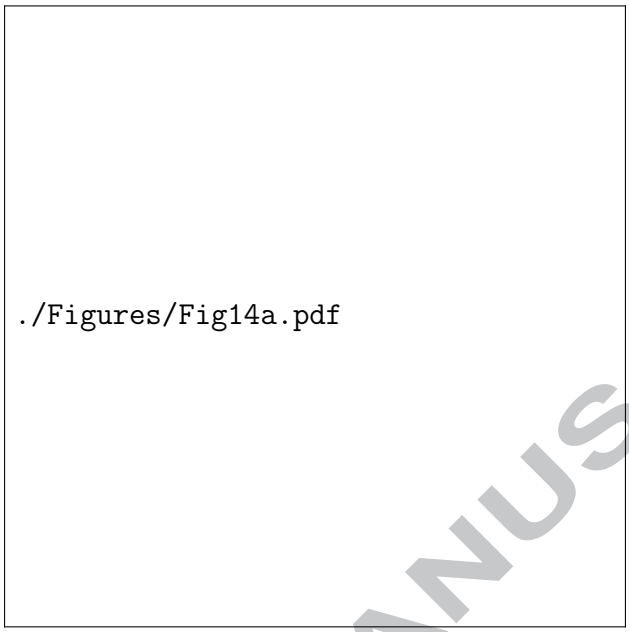

(a)

(b)

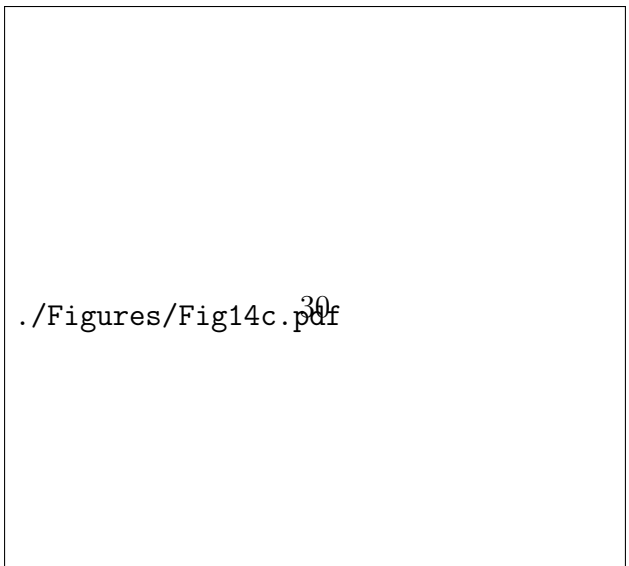

References

[1] J. Nairn, "Matrix microcracking in composites," *Polymer matrix composites*, 2000.

[2] B. Sjögren and L. Berglund, "The effects of matrix and interface on damage in GRP cross-ply laminates," *Composites Science and Technology*, vol. 60, pp. 9–21, 2000.

[3] H. Saito, H. Takeuchi, and I. Kimpara, "Experimental Evaluation of the Damage Growth Restraining in 90 Layer of Thin-ply CFRP Cross-ply Laminates," *Advanced Composite Materials*, vol. 21, pp. 57–66, 2012.

[4] J. Nairn and S. Hu, "The initiation and growth of delaminations induced by matrix microcracks in laminated composites," *International Journal of Fracture*, pp. 1–24, 1992.

[5] M. Kashtalyan and C. Soutis, "Effect of delaminations induced by transverse cracks and splits on stiffness properties of composite laminates," *Composites Part A: Applied Science and Manufacturing*, vol. 31, no. 2, pp. 107–119, 2000.

[6] J.-M. Berthelot, "Transverse cracking and delamination in cross-ply glass-fiber and carbon-fiber reinforced plastic laminates: Static and fatigue loading," *Applied Mechanics Reviews*, vol. 56, no. 1, p. 111, 2003.

[7] Z. Q. Zhou, X. J. Fang, B. N. Cox, and Q. D. Yang, "The evolution of a transverse intra-ply crack coupled to delamination cracks," *International Journal of Fracture*, vol. 165, pp. 77–92, May 2010.

[8] D. Violeau, P. Ladevèze, and G. Lubineau, "Micromodel-based simulations for laminated composites," *Composites Science and Technology*, vol. 69, no. 9, pp. 1364–1371, 2009.

[9] P. Ladevèze and G. Lubineau, "On a damage mesomodel for laminates: micro-meso relationships, possibilities and limits," *Composites Science and Technology*, vol. 61, no. 15, pp. 2149–2158, 2001.

[10] T. Hobbiebrunken, M. Hojo, T. Adachi, C. De Jong, and B. Fiedler, "Evaluation of interfacial strength in CF/epoxies using FEM and in-situ experiments," *Composites Part A: Applied Science and Manufacturing*, vol. 37, no. 12, pp. 2248–2256, 2006.

[11] L. P. Canal, C. González, J. Segurado, and J. LLorca, "Intraply fracture of fiber-reinforced composites: Microscopic mechanisms and modeling," *Composites Science and Technology*, vol. 72, no. 11, pp. 1223–1232, 2012.

[12] D. Mortell, D. Tanner, and C. McCarthy, "In-situ SEM study of transverse cracking and delamination in laminated composite materials," *Composites Science and Technology*, vol. 105, pp. 118–126, Oct. 2014.

[13] D. J. Mortell, D. A. Tanner, and C. T. McCarthy, "An experimental investigation into multi-scale damage progression in laminated composites in bending," *Composite Structures*, vol. 149, pp. –, 2016.

[14] F. Sket, R. Seltzer, J. Molina-Aldareguía, C. Gonzalez, and J. LLorca, "Determination of damage micromechanisms and fracture resistance of glass fiber/epoxy cross-ply laminate by means of X-ray

computed microtomography," *Composites Science and Technology*, vol. 72, pp. 350–359, Jan. 2012.

[15] P. Hine, B. Brew, R. Duckett, and I. Ward, "Failure mechanisms in continuous carbon-fibre reinforced PEEK composites," *Composites Science and Technology*, vol. 35, pp. 31–51, jan 1989.

[16] W. Cantwell, P. Davies, and H. Kausch, "The effect of cooling rate on deformation and fracture in IM6/PEEK composites," *Composite Structures*, vol. 14, pp. 151–171, jan 1990.

[17] M. Lafarie-Frenot and F. Touchard, "Comparative in-plane shear behaviour of long-carbon-fibre composites with thermoset or thermoplastic matrix," *Composites Science and Technology*, vol. 52, pp. 417–425, jan 1994.

[18] T. Q. Li, M. Q. Zhang, K. Zhang, and H. M. Zeng, "The dependence of the fracture toughness of thermoplastic composite laminates on interfacial interaction," *Composites Science and Technology*, vol. 60, pp. 465–476, feb 2000.

[19] L. Berger and W. Cantwell, "Temperature and loading rate effects in the Mode II interlaminar fracture behavior of carbon fiber reinforced PEEK," *Polymer composites*, pp. 271–281, 2001.

[20] S.-L. Gao and J.-K. Kim, "Cooling rate influences in carbon fibre/PEEK composites. Part II: interlaminar fracture toughness," *Composites Part A: Applied Science and Manufacturing*, vol. 32, no. 6, pp. 763–774, 2001.

[21] K. Fujihara, Z.-M. Huang, S. Ramakrishna, and H. Hamada, "Influence of processing conditions on bending property of continuous carbon fiber reinforced PEEK composites," *Composites Science and Technology*, vol. 64, pp. 2525–2534, dec 2004.

[22] L. Ye and K. Friedrich, "Mode I interlaminar fracture of co-mingled yarn based glass/polypropylene composites," *Composites Science and Technology*, vol. 46, no. 2, pp. 187–198, 1993.

[23] L. Ye and K. Friedrich, "Interlaminar fracture (mode II) of commingled yarn-based GF/PP composites," *Journal of Materials Science*, vol. 28, no. 3, pp. 773–780, 1993.

[24] P. Davies and W. J. Cantwell, "Fracture of glass/polypropylene laminates: influence of cooling rate after moulding," vol. 25, no. 9, pp. 869–877, 1994.

[25] M. Bureau, J. Denault, F. Perrin, and I. Dickson, "Crack Propagation in Continuous Glass Fiber/Polypropylene Composites: Matrix Microstructure," *Plastics Failure Analysis and Prevention*, pp. 135–142, 2001.

[26] F. Perrin, M. Bureau, J. Denault, and J. Dickson, "Mode I interlaminar crack propagation in continuous glass fiber/polypropylene composites: temperature and molding condition dependence," *Composites Science and Technology*, vol. 63, pp. 597–607, apr 2003.

[27] K. Jung, D. Kim, H. Kim, S. Park, K. Jhang, and H. Kim, "Finite element analysis of a low-velocity impact test for glass fiber-reinforced polypropylene composites considering mixed-mode interlaminar fracture toughness," *Composite Structures*, vol. 160, pp. 446–456, 2016.

[28] H. Wafai, G. Lubineau, A. Yudhanto, M. Mulle, W. Schijve, and N. Verghese, "Effects of the cooling rate on the shear behavior of continuous glass fiber/impact polypropylene composites (GF-IPP)," *Composites Part A: Applied Science and Manufacturing*, vol. 91, no. Part 1, pp. 41–52, 2016.

[29] "Standard Test Methods for Plane-Strain Fracture Toughness and Strain Energy Release Rate of Plastic Materials 1," *American Society for Testing and Materials (ASTM)*, pp. 1–9, 2013.

[30] S. Pinho, P. Robinson, and L. Iannucci, "Developing a four point bend specimen to measure the mode i intralaminar fracture toughness of unidirectional laminated composites," *Composites Science and Technology*, vol. 69, no. 7, pp. 1303 – 1309, 2009.

[31] "Standard Test Method for Mode I Interlaminar Fracture Toughness of Unidirectional Fiber-Reinforced Polymer Matrix Composites," *American Society for Testing and Materials (ASTM)*, pp. 1–13, 2014.

[32] "Standard Test Method for Determination of the Mode II Interlaminar Fracture Toughness of Unidirectional Fiber-Reinforced Polymer Matrix Composites," *American Society for Testing and Materials (ASTM)*, pp. 1–18, 2014.

[33] A. Yudhanto, G. Lubineau, H. Wafai, M. Mulle, D. Pulungan, R. Yaldiz, and N. Verghese, "Monotonic and cyclic responses of impact polypropylene and continuous glass fiber-reinforced impact polypropylene composites at different strain rates," *Polymer Testing*, vol. 51, pp. 93–100, 2016.

[34] D. M. Montenegro, F. Bernasconi, M. Zogg, M. Gössi, R. Libanori, K. Wegener, and A. R. Studart, "Mode I transverse intralaminar fracture in glass fiber-reinforced polymers with ductile matrices," *Composite Structures*, vol. 165, pp. 65–73, 2017.

[35] R. A. Deblieck, D. van Beek, K. Remerie, and I. M. Ward, "Failure mechanisms in polyolefines: The role of crazing, shear yielding and the entanglement network," *Polymer*, vol. 52, no. 14, pp. 2979–2990, 2011.

[36] M. Benzeggagh and M. Kenane, "Measurement of mixed-mode delamination fracture toughness of unidirectional glass/epoxy composites with mixed-mode bending apparatus," *Composites Science and Technology*, vol. 56, no. 4, pp. 439 – 449, 1996.

[37] K. Leffler, K. Alfredsson, and U. Stigh, "Shear behaviour of adhesive layers," *International Journal of Solids and Structures*, vol. 44, no. 2, pp. 530 – 545, 2007.

[38] D. Stevanovic, *Delamination Properties of a Vinyl-Ester/Glass Fibre Composite Toughened by Particulate-Modified Interlayers*. PhD thesis, Australian National University, September 2010.

[39] D. A. Pulungan, G. Lubineau, A. Yudhanto, R. Yaldiz, and W. Schijve, "Identifying design parameters controlling damage behaviors of fiber-reinforced thermoplastic composites by using micromechanics as a virtual testing tool," *International Journal of Solids and Structures*, vol. 117, pp. 177–190, 2017.

[40] A. Yudhanto, H. Wafai, G. Lubineau, R. Yaldiz, and N. Verghese, "Characterizing the influence of matrix ductility on damage phenomenology in continuous fiber-reinforced thermoplastic laminates un-

dergoing quasi-static indentation," *Composite Structures*, vol. 186, pp. 324 – 334, 2018.

[41] O. Allix, D. Lévêque, and L. Perret, "Identification and forecast of delamination in composite laminates by an interlaminar interface model," *Composites Science and Technology*, vol. 58, no. 5, pp. 671 – 678, 1998.

[42] F. Daghia and C. Cluzel, "The climbing drum peel test: An alternative to the double cantilever beam for the determination of fracture toughness of monolithic laminates," *Composites Part A: Applied Science and Manufacturing*, vol. 78, pp. 70 – 83, 2015.

[43] R. Krueger, "Virtual Crack Closure Technique: History, Approach, and Applications," *Applied Mechanics Reviews*, vol. 57, no. 2, p. 109, 2004.